
Proceedings Paper:
Ansari, S.A., Davidson, J.N. orcid.org/0000-0002-6576-3995 and Foster, M.P. orcid.org/0000-0002-8565-0541 (2020) Analysis, design and modelling of two fully-integrated transformers with segmental magnetic shunt for LLC resonant converters. In: IECON 2020 : The 46th Annual Conference of the IEEE Industrial Electronics Society. IECON 2020 - 46th Annual Conference of the IEEE Industrial Electronics Society, 18-21 Oct 2020, Singapore. Institute of Electrical and Electronics Engineers (IEEE) , pp. 1273-1278. ISBN 9781728154152

https://doi.org/10.1109/iecon43393.2020.9254721

Analysis, Design and Modelling of Two Fully-Integrated Transformers with Segmental Magnetic Shunt for LLC Resonant Converters

Sajad A. Ansari[1], Jonathan N. Davidson[2] and Martin P. Foster[3]
[1, 2, 3]Department of Electronic and Electrical Engineering, The University of Sheffield, Sheffield, UK
[1]SArabAnsari1@sheffield.ac.uk, [2]Jonathan.Davidson@sheffield.ac.uk, [3]M.P.Foster@sheffield.ac.uk

***Abstract*—To achieve a precise, high leakage inductance for an integrated magnetic transformer, a magnetic shunt (based on low-permeability materials) is usually added to the planar transformer. However, high-performance low-permeability power materials are not readily available in the market. Therefore, two new topologies for shunt-inserted planar transformer are proposed in this paper. In the proposed topologies, the magnetic shunts are based on high-permeability materials like ferrite, which is widely available, and use multiple small gaps to approximate a low-permeability material as an alternative to a low-permeability magnetic shunt. The analysis, design and modelling of the proposed planar transformers are presented in detail. It is shown that the magnetizing inductance can be controlled by vertical air gaps and the leakage inductance value can be controlled by the thickness of the shunt. Hence, the desirable leakage inductance and magnetizing inductance values for the integrated transformer can be obtained for use in LLC resonant converters. The theoretical analyses are verified by finite element analysis (FEA) and the AC resistance for the proposed topologies is discussed.**

Keywords—LLC resonant converter; planar Transformer; magnetic shunt; magnetizing inductance; leakage inductance.

I. INTRODUCTION

The pulse-width-modulated converters, such as buck and boost, suffer from high switching losses and cannot provide high efficiency at high switching frequency [1, 2]. Hence, in these converters, high power density cannot be obtained since the switching frequency is limited [3, 4]. Resonant converters benefit from soft switching capability; therefore, they can be operated at high switching frequency to achieve high power density. Amongst resonant converters, the LLC resonant converter is a well-known converter due to its numerous advantages, viz high efficiency at high input voltage range, soft switching capability and integrating magnetic components [5, 6].

Three magnetic components including a resonant inductor, parallel inductor and transformer are needed in an LLC resonant converter. All three magnetic components can be integrated in a single component to increase the power density and efficiency and decrease the cost [7]. Therefore, in recent years, many efforts have been done to integrate magnetics components for LLC resonant converters [8-10]. Integrating magnetic components may be obtained by adding additional windings to the transformer [11]. However, in this structure, the conduction losses are high due to additional windings. Inserting a magnetic shunt which is based on low-permeability materials into a planar transformer is a method to obtain high leakage inductance value. The interest in magnetic shunts has increased recently because the method integrates all the three components in one magnetic core without any additional windings and benefits from advantages of planar transformers, viz high power density, better cooling capability, modularity and manufacturing simplicity. In addition, the leakage inductance can be predicted accurately in this method [12, 13]. The procedure to calculate the leakage inductance for the planar transformer with shunt-inserted is provided in [14]. It is shown that the energies stored in the air gap, windings and insulation layers are far lower than magnetic shunt. In [15], the relationship between air gap and the relative permeability of the shunt and values of leakage and magnetizing inductances are investigated. It is shown that the magnetizing inductance and leakage inductance values can be determined for a limited range of leakage inductance value by controlling the air gap length and the relative permeability of the shunt, respectively.

Even though shunt-inserted planar transformer can provide a high and accurate leakage inductance, the magnetic shunt must be based on low-permeability materials, which are not often readily available in the necessary size and permeability for the applications, and are expensive. Therefore, in order to overcome this issue, two new structures for shunt-inserted planar transformer are proposed in this paper. The proposed shunt-inserted structures are based on high-permeability materials like ferrite, which is widely available in the market, and use small air gaps to approximate a low-permeability material as an alternative to magnetic shunt based on low-permeability materials. The analysis, modelling and design of the proposed integrated magnetic transformers are provided in detail. In addition, the relationship between the magnetizing inductance and leakage inductance values and the characteristic of the shunt based on high-permeability materials is studied. It is shown that the magnetizing inductance has a direct relationship with vertical air gaps while the leakage inductance value is mainly influenced by the thickness of the shunt. The theoretical analysis is confirmed by finite element analysis (FEA) and the AC resistance for the proposed topologies is discussed.

The paper is organized as follows: First, the basic definition of magnetizing and leakage inductances and modelling of both proposed integrated magnetic transformers are presented in section II. In section III, the simulation results are provided. A discussion about the benefits of the proposed segmental shunt compared to the conventional one is presented in section IV. Finally, a brief conclusion can be found in section V.

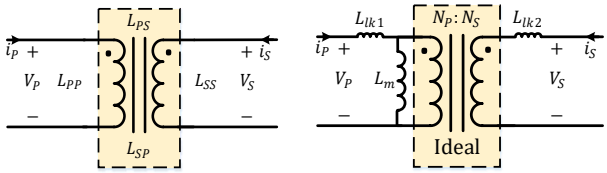

Fig. 1. The equivalent circuit of (a) coupled inductor, (b) transformer.

II. Magnetizing and Leakage Inductance Calculation for the Proposed Topologies

A. Basic definition of magnetizing and leakage inductances

The equivalent circuit of a coupled inductor is shown in Fig. 1(a). The relationship between primary and secondary voltages and currents of this coupled inductor may be expressed by (1) [15, 16].

$$\begin{bmatrix} V_P \\ V_S \end{bmatrix} = \begin{bmatrix} L_{PP} & L_{PS} \\ L_{SP} & L_{SS} \end{bmatrix} \frac{\mathrm{d}}{\mathrm{dt}} \begin{bmatrix} i_P \\ i_S \end{bmatrix} \tag{1}$$

where L_{PS} and L_{SP} are mutual inductances and L_{PP} and L_{SS} are primary and secondary self-inductances, respectively. Another equivalent circuit model of the coupled inductor can be also derived which is shown in Fig. 1(b). The relationship between the voltages and currents of this equivalent circuit may be obtained by (2).

$$\begin{bmatrix} V_P \\ V_S \end{bmatrix} = \begin{bmatrix} L_{lk1} + L_m & \frac{N_S}{N_P} L_m \\ \frac{N_S}{N_P} L_m & L_{lk2} + \frac{N_S^2}{N_P^2} L_m \end{bmatrix} \frac{\mathrm{d}}{\mathrm{dt}} \begin{bmatrix} i_P \\ i_S \end{bmatrix} \tag{2}$$

where N_P and N_S are the total numbers of primary and secondary turns and L_m is the magnetizing inductance of the transformer and may be defined by the following equation.

$$L_m = \frac{N_P}{N_S} L_{PS} \tag{3}$$

The mutual inductance may be calculated as (4).

$$L_{PS} = \frac{N_S}{I_P} \phi_{PS} \tag{4}$$

where ϕ_{PS} is the mutual flux generated by the primary winding. From (3) and (4), the magnetizing inductance can be achieved as follows.

$$L_m = \frac{N_P}{I_P} \phi_{PS} \tag{5}$$

Therefore, in order to obtain the value of the magnetizing inductance, the mutual flux needs to be obtained. The primary self-inductance may be obtained by (6).

$$L_{PP} = \frac{N_P^2}{R} \tag{6}$$

where R is the core reluctance referred to the primary winding. The total leakage inductance value referred to the primary side can be obtained by (7) [15, 16].

$$L_{lk} = 2L_{PP} - 2L_m \tag{7}$$

It is worth noting that in the shunt-inserted planar transformer, the flux of the window area can be compared to the flux of the magnetic shunt [12, 15]. Therefore, to calculate the leakage inductance value, only the leakage inductance caused by the magnetic shunt is considered in this work.

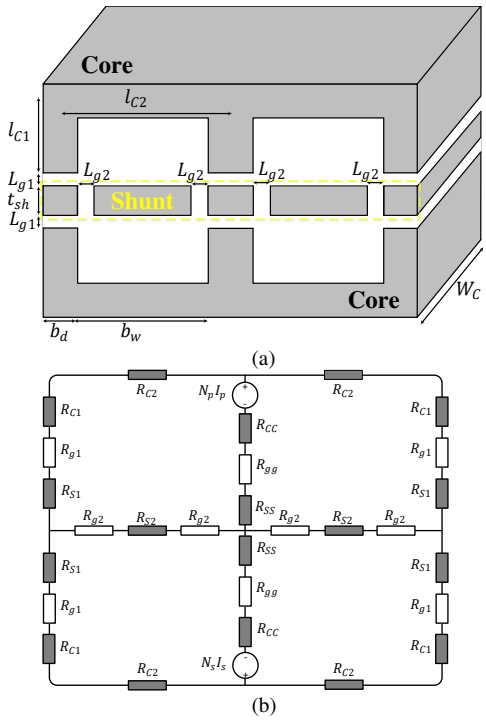

Fig. 2. The proposed integrated magnetic transformer with five-segment shunt. (a) Schematic. (b) Reluctance model.

B. Five-segment magnetic shunt

The schematic of the first proposed shunt-inserted integrated magnetic transformer is shown in Fig. 2 (a). As shown in Fig. 2(a), the magnetic shunt includes four horizontal air gaps in this topology and is based on high-permeability material. In addition, in this topology, the primary and secondary windings are separated in the top and bottom of the magnetic shunt, respectively. The equivalent reluctance model of the proposed topology with a five-segment magnetic shunt is shown in Fig. 2(b). In this model, R_{C1}, R_{C2} and R_{CC} are reluctances of the core, R_{S1}, R_{S2} and R_{SS} are reluctances of the shunt and R_{g1}, R_{g2} and R_{gg} are the reluctances of the air gaps and may be calculated by the following equations.

$$R_{C1} = \frac{l_{c1}}{\mu_0 \mu_r b_d W_c} \tag{8}$$

$$R_{C2} = \frac{l_{c2}}{\mu_0 \mu_r b_d W_c} \tag{9}$$

$$R_{CC} = \frac{l_{c1}}{\mu_0 \mu_r A_c} \tag{10}$$

$$R_{S1} = \frac{t_{sh}}{2\mu_0 \mu_s b_d W_c} \tag{11}$$

$$R_{S2} = \frac{b_w - 2l_{g2}}{\mu_0 \mu_s t_{sh} W_c} \tag{12}$$

$$R_{SS} = \frac{t_{sh}}{2\mu_0 \mu_s A_c} \tag{13}$$

$$R_{g1} = \frac{l_{g1}}{\mu_0 b_d W_c} \tag{14}$$

$$R_{g2} = \frac{l_{g2}}{\mu_0 t_{sh} W_c} \tag{15}$$

$$R_{gg} = \frac{l_{g1}}{\mu_0 A_c} \tag{16}$$

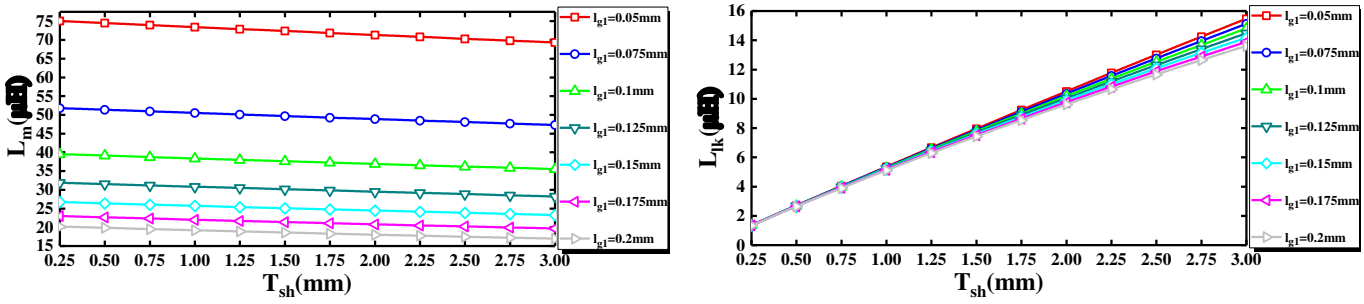

(a) (b)

Fig. 3. The influence of five-segment shunt characteristics on (a) magnetizing inductance, (b) leakage inductances. Core: E32/6/20/R-3F4, shunt: 3F4, L_{g2}=0.46mm and N_P=10.

where μ_0, μ_r and μ_s are the permeability of the air, core and shunt, respectively, A_C is the core effective cross-sectional area and the other quantities are defined in Fig. 2(a).

From the reluctance model given in Fig. 2(b). The mutual flux, ϕ_{PS}, can be obtained using (17).

$$\phi_{PS} = \frac{2N_P I_P (R_{S2} + 2R_{g2})}{R_m (R_m + 2(R_{S2} + 2R_{g2}))} \tag{17}$$

where R_m is defined by (18).

$$R_m = R_{C1} + R_{C2} + 2R_{CC} + R_{S1} + R_{g1} + 2R_{SS} + 2R_{gg} \tag{18}$$

From (5) and (17), the magnetizing inductance value may be obtained by (19).

$$L_m = \frac{2N_P^2 (R_{S2} + 2R_{g2})}{R_m (R_m + 2(R_{S2} + 2R_{g2}))} \tag{19}$$

Again from the reluctance model, the self-inductance of the primary winding may be calculated by (20).

$$L_{PP} = \frac{2N_P^2 (R_{S2} + 2R_{g2} + R_m)}{R_m (R_m + 2(R_{S2} + 2R_{g2}))} \tag{20}$$

Finally, from (7), (19) and (20), the total leakage inductance value referred to the primary side may be obtained by (21).

$$L_{lk} = \frac{4N_p^2}{R_m + 2(R_{S2} + 2R_{g2})} \tag{21}$$

The calculated magnetizing inductance and leakage inductance values versus thickness of the magnetic shunt for different vertical air gaps are shown in Figs. 3(a) and (b), respectively. It is clear that the magnetizing inductance is mainly affected by the vertical air gap and does not change noticeably for different thickness of the shunt. On the other hand, the leakage inductance is mainly affected by the thickness of the shunt and length of the vertical air gap does not have a noticeable influence on it. Therefore, the magnetizing inductance and leakage inductance values can be determined by the length of the vertical air gaps and the thickness of the shunt, respectively.

C. Two-segment magnetic shunt

The schematic of the second proposed shunt-inserted integrated magnetic transformer is shown in Fig. 4 (a). As shown in this figure, even though the magnetic shunt still includes four horizontal air gaps and is based on high-permeability material, it only has two segments which makes the implementation easier, but with the penalty of less volume for windings. The primary and secondary windings are again separated in the top and bottom of the magnetic shunt, respectively. The equivalent reluctance model of the proposed topology with a two-segment magnetic shunt is shown in Fig. 4(b). In this model, R'_{C1}, R'_{C2} and R'_{CC} are still reluctance of the core, R'_{S2} is reluctances of each segment of the shunt and R'_{g1}, R'_{g2} and R'_{gg} are the reluctances of the air gaps and may be calculated by the following equations.

$$R'_{C1} = \frac{l_{c1}}{\mu_0 \mu_r b_d W_c} \tag{22}$$

$$R'_{C2} = \frac{l_{c2}}{\mu_0 \mu_r b_d W_c} \tag{23}$$

$$R'_{CC} = \frac{l_{c1}}{\mu_0 \mu_r A_c} \tag{24}$$

$$R'_{S2} = \frac{b_w - 2l'_{g2}}{\mu_0 \mu_s t_{sh} W_c} \tag{25}$$

$$R'_{g1} = \frac{l'_{g1}}{\mu_0 b_d W_c} \tag{26}$$

$$R'_{g2} = \frac{2l'_{g2}}{\mu_0 t_{sh} W_c} \tag{27}$$

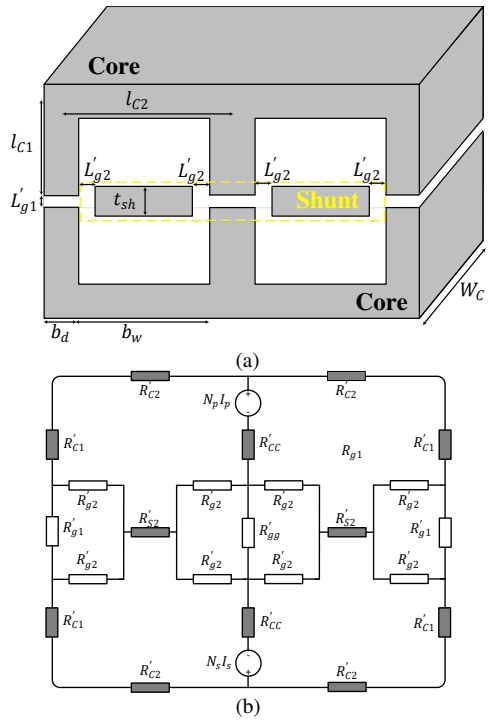

Fig. 4. The proposed integrated magnetic transformer with two-segment shunt. (a) Schematic. (b) Reluctance model.

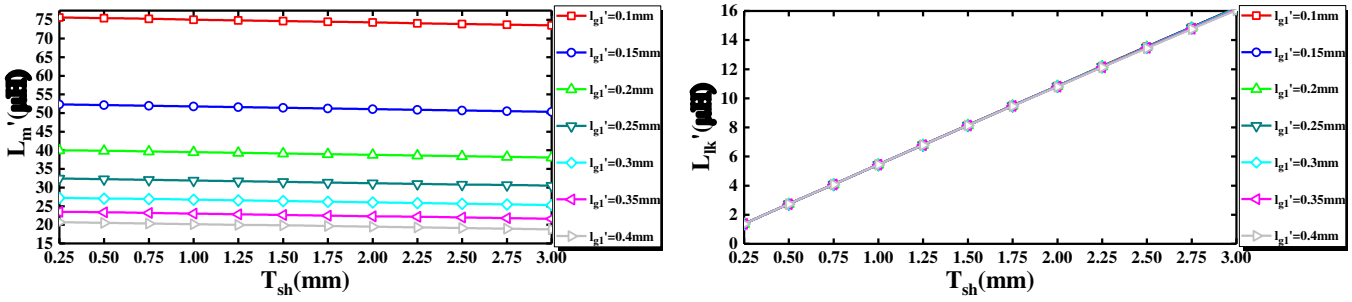

(b) (b)

Fig. 5. The influence of two-segment shunt characteristics on (a) magnetizing inductance, (b) leakage inductance. Core: E32/6/20/R-3F4, shunt: 3F4, L'_{g2}=0.46mm and N_P=10.

$$R'_{gg} = \frac{l'_{g1}}{\mu_0 A_c} \tag{28}$$

where μ_0, μ_r and μ_s are the permeability of the air, core and shunt, respectively, A_C is the core effective cross-sectional area and the rest of the quantities are defined in Fig. 4(a).

From reluctance model indicated in Fig. 4(b), the mutual flux, ϕ'_{PS}, can be obtained by (29).

$$\phi'_{PS} = \frac{2N_P I_P (R'_{S2} + A + B)}{R'_m (R'_m + 2(R'_{S2} + A + B))} \tag{29}$$

where R'_m is defined by (30).

$$R'_m = R_{C1} + R_{C2} + 2R_{CC} + C + D \tag{30}$$

where A, B, C and D are defined as follows.

$$A = \frac{{R'_{g2}}^2}{R'_{g1} + 2R'_{g2}} \tag{31}$$

$$B = \frac{{R'_{g2}}^2}{2R'_{gg} + 2R'_{g2}} \tag{32}$$

$$C = \frac{R'_{g1} R'_{g2}}{R'_{g1} + 2R'_{g2}} \tag{33}$$

$$D = \frac{2R'_{gg} R'_{g2}}{2R'_{gg} + 2R'_{g2}} \tag{34}$$

From (5) and (29), the magnetizing inductance value may be obtained by (35).

$$L'_m = \frac{2N_P^2 (R'_{S2} + A + B)}{R'_m (R'_m + 2(R'_{S2} + A + B))} \tag{35}$$

Again from the reluctance model, the self-inductance of the primary winding may be calculated by (36).

$$L'_{PP} = \frac{2N_P^2 (R'_{S2} + A + B + R'_m)}{R'_m (R'_m + 2(R'_{S2} + A + B))} \tag{36}$$

Finally, from (7), (35) and (36), the total leakage inductance value referred to the primary side may be obtained by (37).

$$L'_{lk} = \frac{4N_p^2}{R'_m + 2(R'_{S2} + A + B)} \tag{37}$$

The calculated magnetizing inductance and leakage inductance values of the second topology versus thickness of the magnetic shunt for different vertical air gaps are shown in Figs. 5(a) and (b), respectively. The magnetizing inductance value is again mainly influenced by the vertical air gaps while it does not change noticeably for different thickness of the shunt. However, the leakage inductance value is highly affected by the thickness of the shunt and length of the vertical air gaps does not have a significant effect on it. Therefore, the magnetizing inductance and leakage inductance values are decoupled and can be designed by the length of the air gaps and the thickness of the shunt, respectively.

III. Simulation Results

In order to confirm the theoretical analysis of both proposed integrated magnetic transformers, the simulation results of both topologies when they are designed at specifications presented in Table I are shown in this section.

The magnetic field intensity of the first and second topologies are shown in Figs. 6(a) and (b), respectively. It is clear that the magnetic field intensity in the horizontal air gaps of the shunt is higher than the window area which proves the fact that leakage inductance value can be calculated from the flux going through the magnetic shunt. In addition, as shown in Figs. 6, the vertical air gaps have the highest magnetic field intensity, which confirms that the magnetizing inductance is highly affected by the length of vertical air gaps. The magnetic flux density vectors of the first and second topologies are shown in Figs. 7(a), and (b), respectively. The main flux goes through the vertical legs and a limited flux which is the leakage flux goes through the magnetic shunts.

The leakage inductances, calculated by the theoretical analysis and measured by simulation, versus the thickness of the magnetic shunt and the length of the vertical air gaps are shown in Figs. 8(a) and (b), respectively. In addition, the magnetizing inductances, calculated by the theoretical analysis and measured by simulation, versus the thickness of the magnetic shunt and the length of the vertical air gaps are shown in Figs. 9(a) and (b), respectively. As shown in Figs. 8 and 9, the simulation results verify the theoretical analysis, and there is only a small discrepancy between the simulation and

Table I. Proposed Topologies' Parameters

Parameter	Symbol	Value
Number of primary turn	N_P	10
Number of secondary turn	N_S	2
Core	C	E32/6/20/R
Permeability of shunt	μ_s	810
Permeability of core	μ_r	810
Vertical air gap for first topology	l_{g1}	0.13 mm
Vertical air gap for second topology	l'_{g1}	0.28 mm
Horizontal air gap for first topology	l_{g2}	0.5 mm
Horizontal air gap for second topology	l'_{g2}	0.5 mm

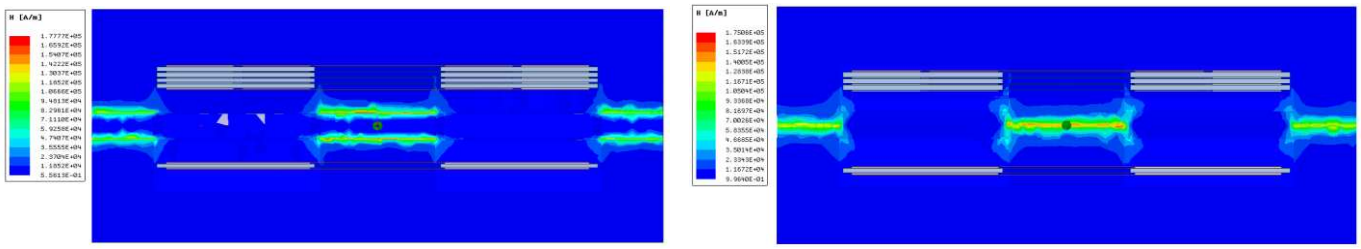

(a) (b)

Fig. 6. Magnetic field intensity of the proposed topologies. (a) Five-segment shunt. (b) Two-segment shunt.

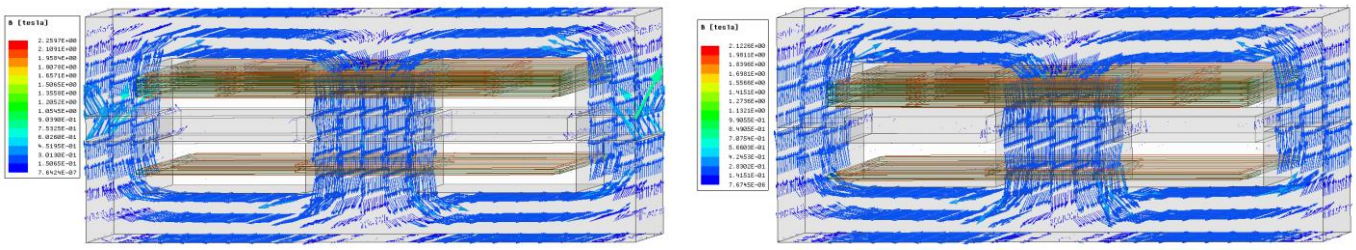

(a) (b)

Fig. 7. Magnetic flux density vector of the proposed topologies. (a) Five-segment shunt. (b) Two-segment shunt.

theoretical results. The assumption that leakage inductance caused by the window area is neglected and the fringing effects explain these discrepancies.

The AC resistance to DC resistance ratio for both the proposed topologies versus operation frequency is shown in Fig. 10. Since the effect of fringing in the five-segment topology is less than two-segment topology and the length between the windings and shunts is higher in five-segment topology, the AC resistance to DC resistance ratio for the five-segment topology is lower. Even though two-segment shunt topology benefits from easier manufacturing and lower volume, it suffers from higher AC resistance.

IV. Discussion

Using a segmental magnetic shunt makes the assembling of the transformer a little bit hard. It is clear that this negative feature of segmental shunt is not a big problem, especially in high production rate, but a fair question is whether using segmental shunt based on the high-permeability material is better than a low-permeability shunt which is not segmental. Therefore, to shed light on this issue, the benefits of the proposed topologies are mentioned as follows.

a) High-permeability materials are cheaper than low-permeability materials.

b) High-permeability material can be found widely in different sizes in the market.

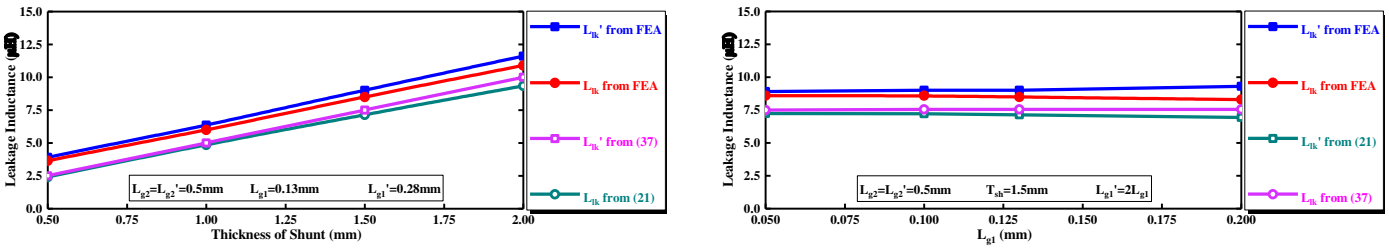

(a) (b)

Fig. 8. Leakage inductance of the proposed topologies versus (a) thickness of shunt, (b) vertical air gap length. Circle for five-segment shunt and square for two-segment shunt.

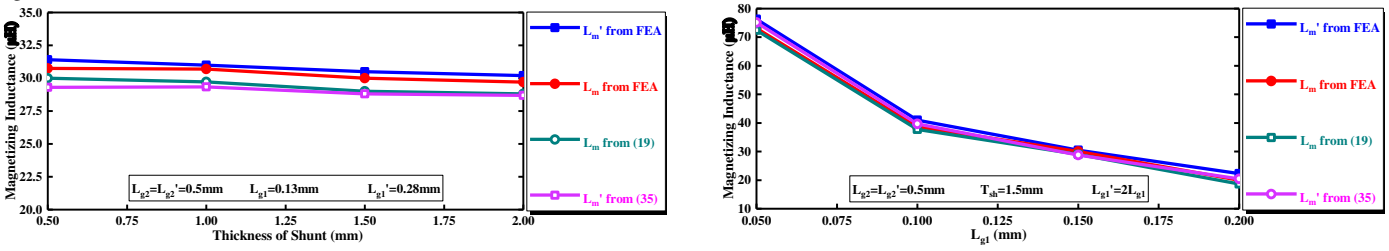

(a) (b)

Fig. 9. Magnetizing inductance of the proposed topologies versus (a) thickness of shunt, (b) vertical air gap length. Circle for five-segment shunt and square for two-segment shunt.

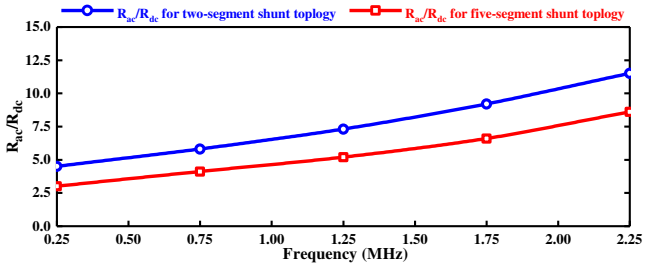

Fig. 10. Ac resistance to DC resistance for both topologies versus frequency.

c) Low-permeability materials are not readily available in the market.

d) Low-permeability materials only can be found in limited relative permeability values in the market, which decreases the flexibility of the design. However, since the permeability of the shunt in the segmental shunts is approximated by the horizontal air gaps, the transformer can be designed with higher flexibility. In other words, changing of the thickness is far more flexible than the changing of the material for different relative permeabilities.

e) In the proposed shunt topologies, the magnetizing inductance and leakage inductance values are decoupled, but when a one-segment shunt based on low-permeability materials is used, they are only decoupled for a limited range of leakage inductance values [15].

In addition, it has been already confirmed in the literature that using a segmental high-permeability core to achieve a quasi-distributed air gap is better than using low-permeability core due to the limitations of the low-permeability materials [17, 18].

V. Conclusion

In this paper, two new topologies for shunt-inserted integrated magnetic transformer are proposed. In the proposed topologies, a segmental shunt based on high-permeability materials is used to approximate a unite shunt with low-permeability material. The analysis and modelling of the proposed topologies are provided in detail. It is shown that the magnetizing inductance and leakage inductance for both topologies are highly influenced by the vertical air gaps and the thickness of the shunt, respectively. The theoretical analysis and design considerations are verified by finite element analysis. In addition, the AC resistance to DC resistance ratio for both of the proposed topologies versus operation frequency is discussed.

References

[1] S. A. Ansari and J. S. Moghani, "A Novel High Voltage Gain Noncoupled Inductor SEPIC Converter," *IEEE Transactions on Industrial Electronics,* vol. 66, no. 9, pp. 7099-7108, 2018.

[2] S. Arab Ansari, J. S. Moghani, and M. Mohammadi, "Analysis and implementation of a new zero current switching flyback inverter," *International Journal of Circuit Theory and Applications,* vol. 47, no. 1, pp. 103-132, 2019.

[3] S. A. Ansari and J. Moghani, "Soft Switching Flyback Inverter for Photovoltaic AC Module Applications," *IET Renewable Power Generation,* vol. 13, no. 13, 2019.

[4] A. Mirzaee, S. Arab Ansari, and J. Shokrollahi Moghani, "Single switch quadratic boost converter with continuous input current for high voltage applications," *International Journal of Circuit Theory and Applications,* vol. 48, no. 4, pp. 587-602, 2020.

[5] R.-L. Lin and W.-C. Ju, "LLC DC/DC resonant converter with PLL control scheme," in *APEC 07-Twenty-Second Annual IEEE Applied Power Electronics Conference and Exposition*, 2007, pp. 1537-1543: IEEE.

[6] R.-L. Lin and C.-W. Lin, "Design criteria for resonant tank of LLC DC-DC resonant converter," in *IECON 2010-36th Annual Conference on IEEE Industrial Electronics Society*, 2010, pp. 427-432: IEEE.

[7] J.-H. Jung, "Bifilar winding of a center-tapped transformer including integrated resonant inductance for LLC resonant converters," *IEEE transactions on power electronics,* vol. 28, no. 2, pp. 615-620, 2012.

[8] S. Stegen and J. Lu, "Structure comparison of high-frequency planar power integrated magnetic circuits," *IEEE transactions on magnetics,* vol. 47, no. 10, pp. 4425-4428, 2011.

[9] Z. Ouyang, O. C. Thomsen, and M. A. Andersen, "Optimal design and tradeoff analysis of planar transformer in high-power DC–DC converters," *IEEE Transactions on Industrial Electronics,* vol. 59, no. 7, pp. 2800-2810, 2010.

[10] W. Liu and J. Van Wyk, "Design of integrated LLCT module for LLC resonant converter," in *Twentieth Annual IEEE Applied Power Electronics Conference and Exposition, 2005. APEC 2005.*, 2005, vol. 1, pp. 362-368: IEEE.

[11] Y. Zhang, D. Xu, K. Mino, and K. Sasagawa, "1MHz-1kW LLC resonant converter with integrated magnetics," in *APEC 07-Twenty-Second Annual IEEE Applied Power Electronics Conference and Exposition*, 2007, pp. 955-961: IEEE.

[12] M. Li, Z. Ouyang, B. Zhao, and M. A. Andersen, "Analysis and modeling of integrated magnetics for LLC resonant converters," in *IECON 2017-43rd Annual Conference of the IEEE Industrial Electronics Society*, 2017, pp. 834-839: IEEE.

[13] Z. Ouyang, W. G. Hurley, and M. A. Andersen, "Improved Analysis and Modeling of Leakage Inductance for Planar Transformers," *IEEE Journal of Emerging and Selected Topics in Power Electronics,* vol. 7, no. 4, pp. 2225-2231, 2018.

[14] J. Zhang, Z. Ouyang, M. C. Duffy, M. A. Andersen, and W. G. Hurley, "Leakage inductance calculation for planar transformers with a magnetic shunt," *IEEE Transactions on Industry Applications,* vol. 50, no. 6, pp. 4107-4112, 2014.

[15] A. Taylor, J. Lu, L. Zhu, K. H. Bai, M. McAmmond, and A. Brown, "Comparison of SiC MOSFET-based and GaN HEMT-based high-efficiency high-power-density 7.2 kW EV battery chargers," *IET Power Electronics,* vol. 11, no. 11, pp. 1849-1857, 2018.

[16] S. De Simone, C. Adragna, and C. Spini, "Design guideline for magnetic integration in LLC resonant converters," in *2008 International Symposium on Power Electronics, Electrical Drives, Automation and Motion*, 2008, pp. 950-957: IEEE.

[17] J. Hu and C. R. Sullivan, "The quasi-distributed gap technique for planar inductors: Design guidelines," in *IAS'97. Conference Record of the 1997 IEEE Industry Applications Conference Thirty-Second IAS Annual Meeting*, 1997, vol. 2, pp. 1147-1152: IEEE.

[18] J. Hu and C. R. Sullivan, "AC resistance of planar power inductors and the quasidistributed gap technique," *IEEE Transactions on Power Electronics,* vol. 16, no. 4, pp. 558-567, 2001.